

# COLOURING MECHANISMS IN RUTILE-BASED CERAMIC PIGMENTS

Francesco Matteucci<sup>(2)</sup>, Giuseppe Cruciani<sup>(1)</sup>, Michele Dondi<sup>(2)</sup>, Guia Guarini<sup>(2)</sup>,  
Marianosa Raimondo<sup>(2)</sup>

<sup>(1)</sup>Earth Science Department, University of Ferrara, Ferrara (Italy)

<sup>(2)</sup>ISTEC – CNR, Institute of Science and Technology for Ceramics, Faenza (Italy)

## ABSTRACT

*The excellent optical features and the high refractive index of titanium dioxide - TiO<sub>2</sub> - make it a valuable pigment and opacifier for a broad range of applications in ceramics, paints, plastic goods, inks and paper. TiO<sub>2</sub> in the form of anatase progressively convert to rutile on heating. The temperature and the rate of the anatase-to-rutile transformation vary in quite a wide range, depending on several factors such as amount and nature of impurities, deviation of the stoichiometry, atmosphere, contact angle of the powders, etc. The presence of a chromophore ion entering the TiO<sub>2</sub> structure determines the presence of a crystal field, whose effects give rise to different colouring patterns. In this work the synthesis of 12 different compositions with the stoichiometry Ti<sub>1-2x</sub>A<sub>x</sub>B<sub>x</sub>O<sub>2</sub> - where A = Cr, Mn, Ni, V and B = Nb, Sb, W (x=0.03) was performed. The characterization of the pigments was achieved combining X-ray powder diffraction, Rietveld refinement and UV-Vis-NIR spectroscopy data in order to clarify the contribution of each chromophore ion to the crystal field strength and the role played by the counter-ion. Moreover, for each dopant ion an attempt of explaining the colouring mechanisms was done.*

## 1. INTRODUCTION

Titanium dioxide -  $\text{TiO}_2$  - can crystallize in different polymorphs: rutile and anatase (tetragonal), brookite (orthorhombic). Rutile is the only stable phase, while the two metastable phases anatase and brookite irreversibly transform to rutile on heating. Titanium dioxide in the form of anatase is a white powder with high opacity, brilliant whiteness, excellent covering power, chemical and physical resistance. These excellent optical features, coupled with the high refractive index, made it a valuable pigment and opacifier for a broad range of applications in ceramics, paints, plastic goods, inks and paper <sup>[1]</sup>.

The opacifying power of the  $\text{TiO}_2$  is progressively reduced with the anatase-to-rutile transformation which can take place at very different temperatures between 400 and 1000°C, depending on several factors <sup>[2-6]</sup>. The presence of a  $\text{Ti}^{4+}$ -oxygen charge transfer band occurring in the near UV, makes the Ti-, oxygen-based compounds colourless. The charge transfer band partially shifts to the visible region when the anatase-to-rutile transformation occurs, so that a typical cream colour arises. In fact, the charge transfer band of anatase, centred at about 29800  $\text{cm}^{-1}$ , in the case of rutile is progressively shifted towards 26500  $\text{cm}^{-1}$  approaching the visible region <sup>[7]</sup>. The contemporary presence of a chromophore ion entering the  $\text{TiO}_2$  structure determines the presence of a crystal field, whose effects give rise to different colouring patterns.

In the field of traditional ceramic, the use of pigments with the rutile structure is by now well founded. In particular, these pigments are widely used as body stains in the production of porcelain stoneware tiles <sup>[6]</sup>, while their utilization as glaze colour is more limited due to the low solubility and chemical stability in many glassy matrices which brings about a fast decreasing of the colouring power during the industrial thermal process. Notwithstanding a rather wide range of colours could be obtained with the rutile structure, only two pigments are currently produced at industrial level: orange  $\text{Ti}_{1-2x}\text{Cr}_x\text{Sb}_x\text{O}_2$  <sup>[9]</sup> and tobacco  $\text{Ti}_{1-2x}\text{Cr}_x\text{W}_x\text{O}_2$  <sup>[10]</sup>. According to the DCMA list <sup>[9]</sup>, other rutile pigments can be obtained with different chromophore ions, such as Ni (yellow), Mn and V (brown), using Sb, W or Nb as counter-ions in order to balance the charge mismatch due to the  $\text{Ti}^{4+}$  replacement by the 3<sup>+</sup> doping ions.

In this work the anatase-to-rutile transformation was deeply investigated in order to ascertain the effects of different variables on the conversion rate. The transformation rate, in fact, is very sensitive to the reaction temperature, the deviation of the stoichiometry, the amount and type of additives, atmosphere, contact angle of the powders, etc.

In the literature the influence played by these parameters has been extensively evaluated <sup>[2-6]</sup> and the effect of different impurities content on the anatase-to-rutile transformation is well known. According to these studies, alkaline (K, Na, Li) and transition metals ions (Fe, Mn, Cr, etc.), having a valence lower than 4<sup>+</sup>, are believed to accelerate the anatase-to-rutile transformation since they contribute to increase the oxygen vacancies which act as sites for the rutile nucleation <sup>[12-15]</sup>. On the contrary, the influence of the cationic radius is still under debate [15], as well as the role played by the presence of those counter-ions (Sb, Nb, Ta, etc) necessary to balance the charge mismatch due to the  $\text{Ti}^{4+}$  replacement by 3<sup>+</sup> dopants. Moreover, just few literature data concern with the colorimetric features of these structures <sup>[9,16]</sup>, as well as with the colouring mechanisms and the interpretation of the corresponding UV-VIS patterns <sup>[16, 17]</sup>.

The aim of this work is to better understand the mechanisms of coloration of rutile pigments having the following stoichiometry:  $Ti_{1-2x}A_xB_xO_2$  - where A (chromophore ion) = Cr, Mn, Ni, V and B (counter-ion) = Nb, Sb, W, with  $x=0.03$ . The characterization of the pigments was accomplished by combining X-ray powder diffraction, Rietveld refinement and UV-Vis-NIR spectroscopy data in order to determine the contribution of each chromophore ion to the crystal field strength and the role played by the counter-ion.

## 2. MATERIALS AND METHODS

A set of 12 compositions, designed with the following stoichiometry:  $Ti_{1-2x}A_xB_xO_2$  - where A = Cr, Mn, Ni, V and B = Nb, Sb, W, with  $x=0.03$  - was prepared through the ceramic method. The titanium dioxide used as raw material was in the form of anatase, while the following oxides were used as dopants source:  $Cr_2O_3$ ,  $Mn_2O_3$ , NiO,  $V_2O_5$ ,  $Nb_2O_5$ ,  $Sb_2O_3$ ,  $WO_3$  (reagent grade quality of 99,9%) having an average particle size of 20-30 $\mu$ m. Pigments were prepared by wet mixing in porcelain jar-mill for 10', drying at  $105 \pm 5^\circ C$  and firing in alumina crucibles at five different temperature: 700, 800, 900, 1000, 1100 $^\circ C$  (200 $^\circ C/h$  heating rate and 1h soaking time). Different samples were labelled with two letters: the first one indicating the metal transition ion, where C, N, M and V stand for chromium, nickel, manganese and vanadium, respectively; the second one indicating the counter-ion, where N, S and W stand for niobium, antimony and tungsten, respectively. The number following the letters indicates the maximum firing temperature, where 7, 8, 9, 10 and 11 stand for 700, 800, 900, 1000 and 1100  $^\circ C$ , respectively. Un-doped rutile reference samples were also prepared by firing pure anatase (AA).

The synthesized pigments were ground in agate mortar up to a particle size distribution with  $\Phi_{50}$  of 10  $\mu$ m. The resulting powders were characterized by combining X-ray powder diffraction (XRPD) and UV-Vis-NIR spectroscopy data. Powder diffraction patterns were collected using a Philips PW 1820/00 diffractometer, equipped with a diffracted beam monochromator ( $CuK_{\alpha 1,2}$  radiation), and the data were obtained in the following conditions:  $2\theta$  range = 15-130 $^\circ$ ; stepsize = 0.02; time/step = 10 sec. Crystal structure refinement of samples fired at 1100  $^\circ C$  were performed by the Rietveld method. A complete description of refinement details and discussion of structural results will be given elsewhere<sup>[18]</sup>. Some selected results (unit cell parameters, weight fractions and bond lengths refined for rutile) are reported in Table 1 in order to facilitate discussion in combination with the results from UV-Vis-NIR spectroscopy. UV-visible-NIR spectra and CIE-Lab colour coordinates ( $L^*$ ,  $a^*$ ,  $b^*$ ) were obtained at room temperature with a Perkin Elmer  $\lambda 35$  spectrophotometer. Data were registered from 200 to 1100 nm, using an integrating sphere,  $BaSO_4$  as white reference and D65 as standard illuminant.

## 3. RESULTS AND DISCUSSION

Two competitive mechanisms are responsible for the coloration of the rutile structure containing foreign ions: the charge transfer between titanium and oxygen and the crystal field produced by the presence of the ions.

The charge transfer band for oxygen compound of  $Ti^{4+}$  occurs in the near UV, making the anatase structure colourless. When the anatase-to-rutile transformation takes place, the wavelength of the charge transfer band partially shifts to the visible

region so that a typical pale yellow colour arises. In fact, the charge transfer band of anatase, centred at about 29800 cm<sup>-1</sup>, in the case of rutile is progressively shifted towards 26500 cm<sup>-1</sup> approaching the visible region [7]. In figure 2 the progressive shifting of the absorption band of anatase towards the visible region is shown as a function of the anatase-to-rutile transformation.

Sample	Rutile amount wt. fr.	Cell parameters			(Ti,Me)-O bond distance		
		a=b Å	c Å	Volume Å <sup>3</sup>	[2x] (Å)	[4x] (Å)	Mean (Å)
AA11	1.000	4.595	2.959	62.47	1.979	1.950	1.9596
CN11	0.999	4.597	2.962	62.60	1.979	1.952	1.9610
CS11	1.000	4.595	2.964	62.58	1.976	1.954	1.9612
CW11	0.996	4.593	2.958	62.41	1.972	1.954	1.9597
MN11	1.000	4.597	2.960	62.56	1.986	1.946	1.9595
MS11	1.000	4.595	2.962	62.56	1.976	1.952	1.9601
MW11	0.984	4.598	2.957	62.54	1.980	1.950	1.9602
NN11	0.986	4.597	2.962	62.60	1.977	1.953	1.9613
NS11	1.000	4.596	2.964	62.62	1.975	1.955	1.9617
NW11	1.000	4.598	2.960	62.56	1.975	1.954	1.9611
VN11	1.000	4.593	2.961	62.46	1.973	1.954	1.9601
VS11	1.000	4.593	2.963	62.49	1.972	1.955	1.9606
VW11	0.958	4.592	2.958	62.38	1.957	1.962	1.9608

Table 1. Cell parameters and metal-oxygen distances of pigments fired at 1100°C from Rietveld refinements.

As known from the literature [2-6], the rate of the anatase-to-rutile transition depends on many variables such as the synthesis method of the anatase, its degree of crystallinity, the furnace atmosphere, the presence of different impurities, etc. In particular, the presence of dopant ions can accelerate or retard the transition, according to their valence state. In fact, it has been suggested that those ions with a valence lower than 4+ promote the anatase-to-rutile transformation since they contribute to increase the oxygen anionic vacancies which act as sites for the rutile nucleation [12-15]; on the contrary, ions with a valence higher than 4+ delay the transition, reducing the oxygen vacancies concentration.

As shown in Figure 2, the influence of the metal transition ions on the anatase-to-rutile transition is different in terms of rate, but all of them accelerate the reaction; in particular, V is the most effective ion in promoting the transition, followed by Cr, Ni and Mn. In the case of V, it can be observed that the anatase-to-rutile transition takes place at a temperature of about 200°C lower than the temperature of the pure anatase transition. Besides, the influence of Sb and W and the known retarding effect of Nb [6] are completely hidden by the effect of the transition metal ions. Furthermore, the transition rate is probably influenced by the presence of secondary phases; in fact, the lowest transition rates of samples CN11 and MW11 correspond to the presence of CrNbO<sub>4</sub> and MnWO<sub>4</sub> as secondary phases, respectively.

The colour of the pigments depends on the rutile content of the samples; in fact, in samples doped with Cr (figure 3A) and Ni (figure 3B) the colour intensity increases proportionally to the rutile amount (Table 2).

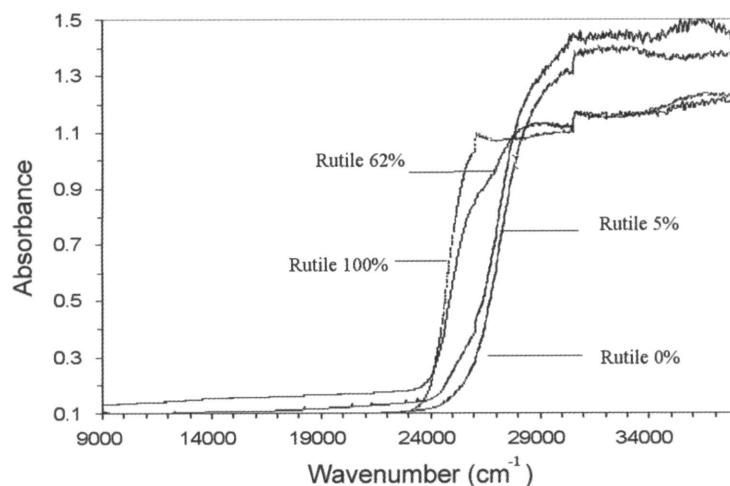


Figure 1. UV-Vis-NIR spectra of TiO<sub>2</sub> samples showing the shift of the charge transfer band as a function of the rutile fraction.

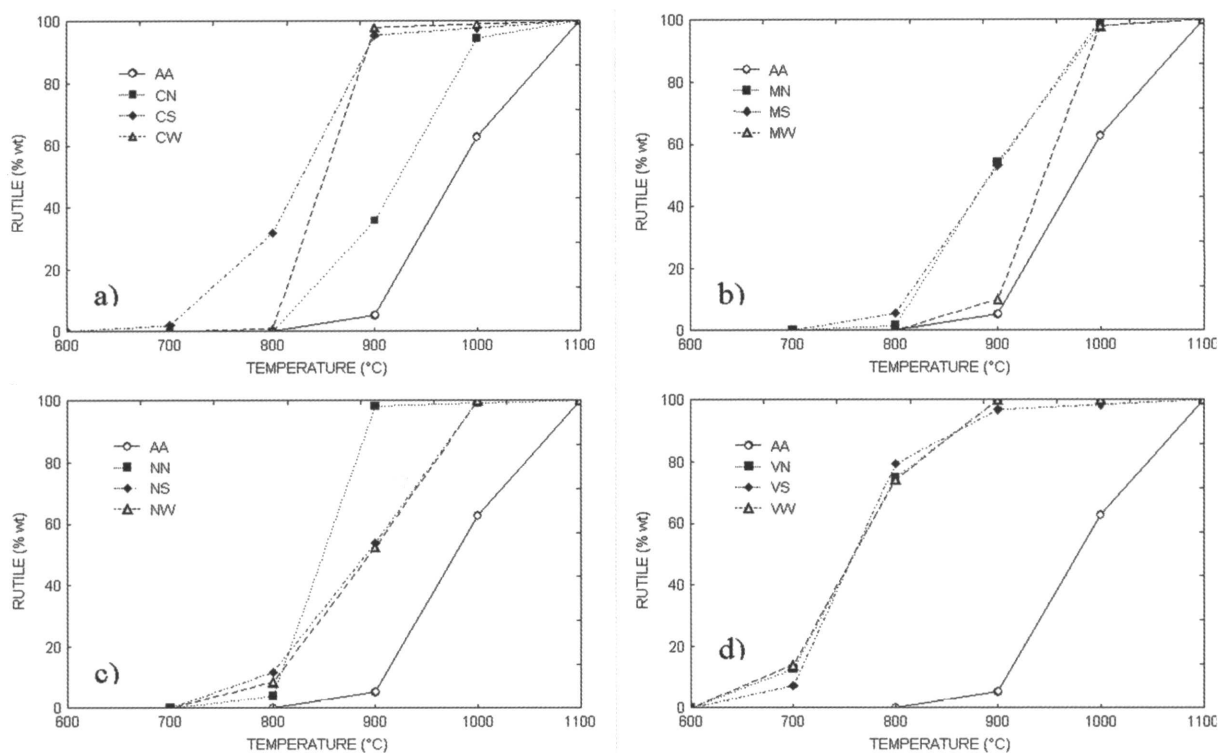


Figure 2 . Effect exerted by a) chromium b) manganese c) nickel d) vanadium on the anatase-to-rutile transition.

Nevertheless, as it can be observed in Table 2 and Figure 3, the phase composition is not the only parameter controlling the pigment colour. In fact, in the samples fired at 1000°C the Cielab a\*-b\* parameters and the colour purity increase with the rutile percentage, while the same parameters suffer of a further increment in the samples fired at 1100°C, although the amount of rutile is nearly the same.

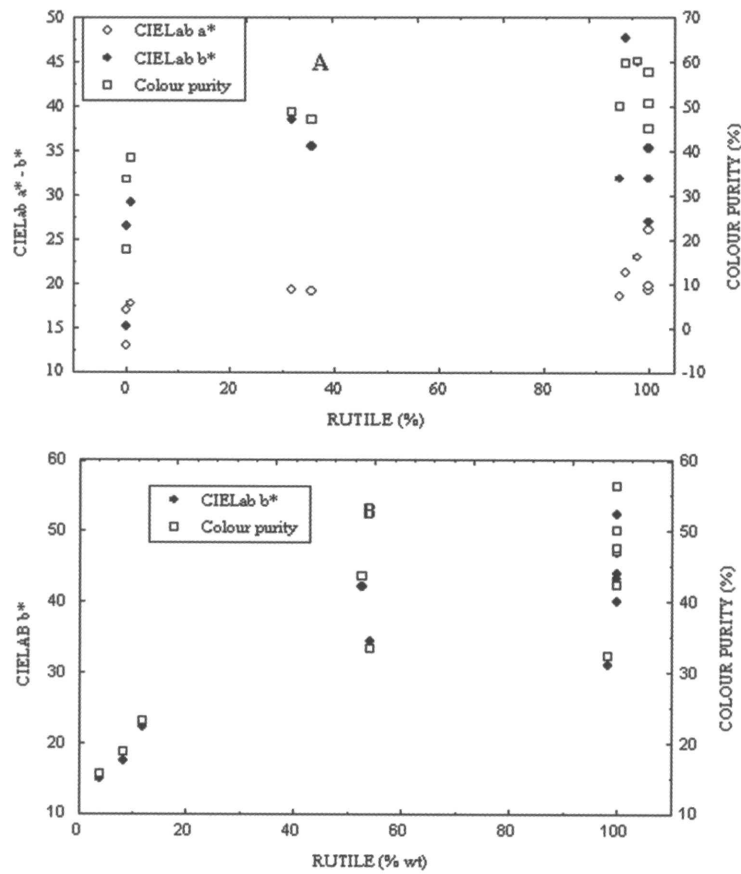


Figure 3. CieLab  $a^* - b^*$  values and colour purity versus the rutile amount in A) Cr doped and B) Ni doped samples.

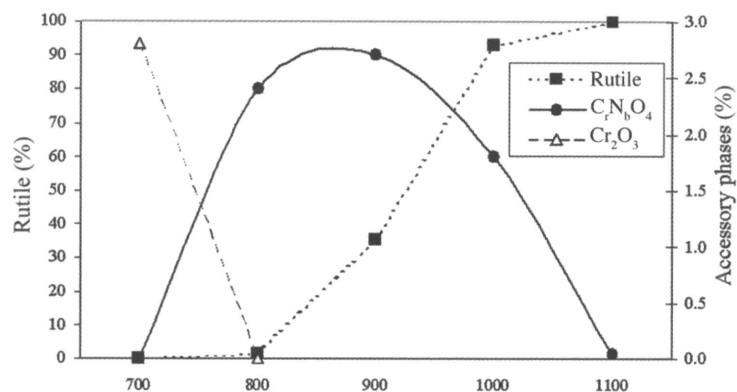


Figure 4. Variation of the phase composition of sample CN as a function of the maximum firing temperature

Muestra	L*	a*	b*	Pureza de color	Fases accesorias	Muestra	L*	a*	b*	Pureza de color	Fases accesorias
AA8	92.25	0.01	2.14	-	Ninguna	NN8	86.00	-3.20	14.82	15.72	NiNb <sub>2</sub> O <sub>6</sub>
AA9	90.10	-0.05	2.60	-	Ninguna	NN9	87.47	-6.17	31.07	32.33	NiNb <sub>2</sub> O <sub>6</sub> – NiTiO <sub>3</sub>
AA10	86.25	-0.36	2.55	-	Ninguna	NN11	81.98	-5.49	43.21	47.12	Ninguna
AA11	92.98	-0.93	4.07	-	Ninguna	NS8	87.82	-5.66	22.33	23.06	Sb <sub>2</sub> O <sub>3</sub> – NiO
CN7	76.11	-4.10	15.14	17.59	Cr <sub>2</sub> O <sub>3</sub> - Nb <sub>2</sub> O <sub>5</sub>	NS9	86.83	-7.03	34.40	33.48	Sb <sub>2</sub> O <sub>3</sub> – NiO
CN8	73.62	3.84	26.38	33.44	CrNbO <sub>4</sub>	NS10	85.51	-6.94	40.13	42.27	NiO
CN9	68.73	8.32	35.53	47.17	CrNbO <sub>4</sub>	NS11	83.24	-6.10	46.90	50.18	NiO - NiTiO <sub>3</sub>
CN10	56.64	7.46	31.91	49.93	CrNbO <sub>4</sub>	NW8	86.32	-2.55	17.43	18.65	NiWO <sub>4</sub>
CN11	52.77	8.77	27.11	45.14	CrNbO <sub>4</sub>	NW9	87.81	-4.68	42.14	43.72	NiWO <sub>4</sub>
CS8	72.60	8.79	38.49	48.67	Ninguna	NW10	83.34	-4.02	44.03	47.56	NiWO <sub>4</sub>
CS9	71.49	12.55	47.68	59.53	Ninguna	NW11	82.14	-2.66	52.30	56.39	NiO
CS11	54.81	9.58	31.92	50.78	Ninguna	VN7	56.46	2.92	19.52	30.72	Ninguna
CW8	70.69	5.37	29.23	38.27	WO <sub>3</sub>	VN8	44.54	3.12	8.34	16.53	Ninguna
CW9	66.27	16.17	45.02	60.38	WO <sub>3</sub>	VN9	38.03	2.74	6.75	16.21	Ninguna
CW11	54.64	22.32	35.35	57.75	WO <sub>3</sub>	VN11	30.67	3.24	6.43	16.88	Ti <sub>5</sub> O <sub>9</sub>
MN8	74.64	1.22	10.32	13.09	Mn <sub>2</sub> O <sub>3</sub> – MnNb <sub>2</sub> O <sub>4</sub>	VS7	73.79	-1.42	20.11	24.77	V <sub>2</sub> O <sub>3</sub>
MN9	58.91	10.17	17.63	28.81	Mn <sub>2</sub> O <sub>3</sub> – MnNb <sub>2</sub> O <sub>6</sub>	VS8	49.58	3.21	7.87	14.50	SbVO <sub>4</sub> - V <sub>2</sub> O <sub>3</sub>
MN10	47.91	13.97	18.67	36.26	Mn <sub>2</sub> TiO <sub>4</sub>	VS9	45.64	3.03	5.77	11.57	Ninguna
MN11	35.35	7.77	10.67	26.13	Mn <sub>2</sub> TiO <sub>4</sub>	VS11	32.98	2.22	5.30	13.11	Ti <sub>5</sub> O <sub>9</sub>
MS8	69.45	3.66	8.57	12.18	Mn <sub>2</sub> O <sub>3</sub>	VW7	52.69	5.07	17.63	29.95	WO <sub>3</sub>
MS9	57.65	6.18	6.06	11.02	Mn <sub>2</sub> O <sub>3</sub> – MnSb <sub>2</sub> O <sub>6</sub>	VW8	44.69	4.54	10.69	21.23	WO <sub>3</sub>
MS10	52.06	10.19	11.89	22.52	Mn <sub>2</sub> O <sub>3</sub> – MnSb <sub>2</sub> O <sub>6</sub>	VW9	39.87	3.84	9.50	20.44	WO <sub>3</sub>
MS11	35.97	6.39	7.27	18.20	Ninguna	VW11	29.44	0.53	0.01	-0.62	WO <sub>3</sub> – Ti <sub>5</sub> O <sub>9</sub>
MW9	68.93	5.29	14.42	20.28	MnWO <sub>4</sub>						
MW10	52.88	10.66	11.78	22.22	MnWO <sub>4</sub>						

Table 2. Colorimetric characteristics (CIELab a\*b\*; colour purity) of pigments fired at different temperatures and accessory phases as detected by XRPD.

Concerning the effect of the different transition metal ions introduced in the rutile structure on the crystal field, from the analysis of UV-Vis-NIR spectra (Figure 5) it can be observed that the characteristic absorbance peaks of each ion are almost completely hidden by the charge transfer band of rutile. Nevertheless, looking more in detail at the absorbance spectra and referring to the Tanabe-Sugano diagrams<sup>[19]</sup>, for each transition metal the following information on the crystal field effects can be inferred:

**Chromium** (Figure 5a): the presence of Cr<sup>3+</sup> (configuration d<sup>3</sup>) in the rutile structure gives rise to the two spin forbidden <sup>4</sup>A<sub>2</sub>→<sup>2</sup>E and <sup>4</sup>A<sub>2</sub>→<sup>2</sup>T<sub>1</sub> transitions, whose wavelengths do not depend on the crystalline structure, centred at about 13000-14000 cm<sup>-1</sup>; the <sup>4</sup>A<sub>2</sub>→<sup>4</sup>T<sub>2</sub> transition produces a broad absorbance peak in the 24000-25000 cm<sup>-1</sup> range.

**Manganese** (Figure 5b): the presence of Mn in the rutile structure gives rise to a broad absorbance peak between 21000 and 23000 cm<sup>-1</sup>, but it is not clear if it is due to the presence of Mn<sup>3+</sup> (configuration d<sup>4</sup>, <sup>5</sup>E<sub>g</sub>→<sup>5</sup>T<sub>2g</sub> transition) or Mn<sup>2+</sup> (configuration d<sup>5</sup>, <sup>6</sup>A<sub>1</sub>→<sup>4</sup>E, <sup>4</sup>A transition).

As reported in Table 2,  $MnNb_2O_6$  crystallizes in samples fired at  $700^\circ C$ , while at  $900^\circ C$  unreacted  $Mn_2O_3$  is still present. According to Shannon ionic radii values [20],  $Ti^{4+}$  in the octahedral coordination has a ionic radius of  $0.60 \text{ \AA}$  so that the most reasonable valence of Mn entering the structure should be  $3+$  (ionic radius of  $0.64 \text{ \AA}$  compared with  $0.83 \text{ \AA}$  ionic radius of  $Mn^{2+}$ ). However, this latter conclusion can not be completely supported by the spectral evidences.

**Nickel** (Figure 5c): the existence of secondary phases in which Ni has a  $2+$  valence has been detected by XRPD (Table 2). From the analysis of UV-Vis-NIR spectra it is possible to observe two main absorbance peaks at about  $12000\text{-}14000 \text{ cm}^{-1}$  and  $22000\text{-}24000 \text{ cm}^{-1}$ , reasonably explained with the  ${}^3A_2 \rightarrow {}^3T_1({}^3F)$  and  ${}^3A_2 \rightarrow {}^3T_1({}^3P)$  transitions of  $Ni^{2+}$  in  $3d^8$  configuration. Nevertheless, referring to ionic radii values, it cannot be excluded the presence of  $Ni^{3+}$  in the rutile structure since it has the same ionic radius of  $Ti^{4+}$ , while the difference between  $Ni^{2+}$  and  $Ti^{4+}$  is  $0.09 \text{ \AA}$ .

**Vanadium** (Figure 5d): vanadium accelerates the anatase-to-rutile transition and only unreacted  $WO_3$  is present as secondary phase. From the analysis of UV-Vis-NIR spectra, the existence can be remarked of a wide absorbance band in the  $14000\text{-}24000 \text{ cm}^{-1}$  region. This band can be explained with the superimposition of the absorbance effect of the  ${}^3T_1 \rightarrow {}^3T_2$  transition (at about  $17000 \text{ cm}^{-1}$ ) due to  $V^{3+}$  in the  $d^2$  configuration and the  ${}^3T_1({}^3F) \rightarrow {}^3T_1({}^3P)$  transition (at about  $24000 \text{ cm}^{-1}$ ) of  $V^{4+}$  in the  $d^1$  configuration. The presence of vanadium with a  $4+$  valence state could also explain the continuous absorbance in the  $19000\text{-}22000 \text{ cm}^{-1}$  region due to the  ${}^2T_2 \rightarrow {}^2E$  transition (at about  $20000 \text{ cm}^{-1}$ ).

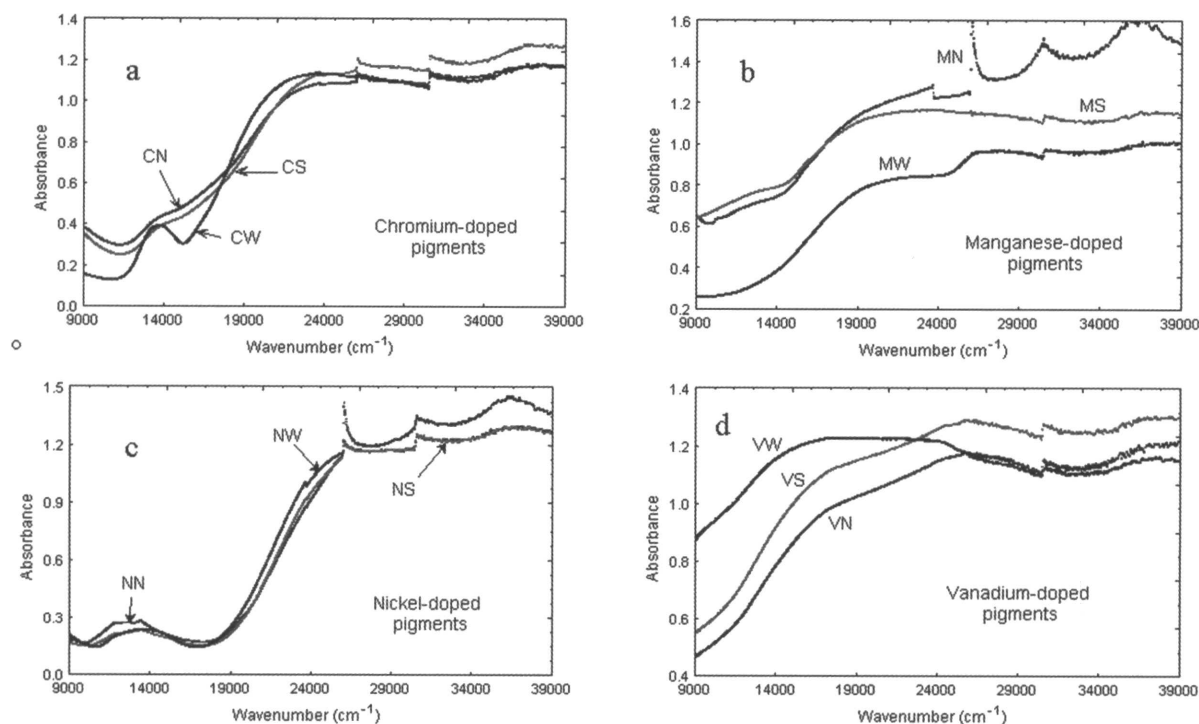


Figure 5. UV-Vis-NIR spectra of rutile doped pigments fired at  $1100^\circ C$ .

As far as the structural data are concerned, the variations of the unit cell dimensions and bond lengths of rutile from Rietveld refinements are given on Figure 6 and Figure 7, respectively.

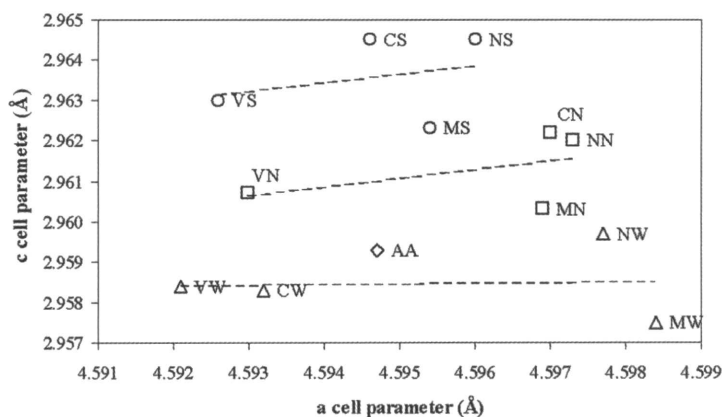


Figure 6. Plot of the *c* cell parameter vs. the *a* cell parameter of rutile doped pigments fired at 1100 °C.

Preliminary evaluation of unit cell parameters and bond lengths variations as directly related to the changes of the average ionic radii, calculated for the different (nominal) compositions by assuming 3+ and 5+ valence states for the A and B ions respectively, did not show any straightforward correlation. This implies that the assumption of a given valence state for ions A and B, simply based on charge balance considerations is not a satisfactory approximation. Furthermore, it suggests that mixed valence states for each ion cannot be ruled out. By analysing the variation of the *c* vs. *a* unit cell dimensions, some trends can be observed. All data points can be viewed as underlying along three series, related to the three different counter-ions (W, Nb, Sb), showing nearly parallel trends of the almost constant *c* cell dimension (see Figure 7). The three series exhibit an increase of the average *c* dimension with the sequence  $W < Nb < Sb$ . This sequence might be explained with the increasing ionic radius of the counter-ion ( $W^{5+}$ : 0.62 Å <  $Nb^{5+}$ : 0.64 Å <  $Sb^{3+,5+}$ : 0.68 Å) by assuming that Sb is incorporated with both the 3+ (0.60 Å) and 5+ (0.76 Å) valence states. It should be noted that the substitution of  $Ti^{4+}$  by  $Sb^{5+}$  would be favoured by their similarity of ionic radius (0.61 Å for  $Ti^{4+}$  vs. 0.60 Å for  $Sb^{5+}$ ), however the presence of  $Sb^{3+}$  (0.74 Å) is supported by previous literature reports [15]. It is likely that the ratio of the 3+ and 5+ valence states for Sb changes along the “Sb-series” according to charge balance requirements for each different A ion. Concerning the effects of the A ions on the unit cell dimensions, it can be suggested that they mainly affect the *a* unit cell dimension. The lengthening of the *a* cell parameter can tentatively be explained by the general increase of the ionic size of A ions according to a sequence  $V < Cr < Mn < Ni$  as observed in particular for the “Sb-series”. This might be converted into a sequence of increasing ionic radius of the A ion by assuming a given valence (and the corresponding radius) for each ion:  $V^{4+}$  (0.58 Å) <  $Cr^{3+}$  (0.62 Å) <  $Mn^{3+}$  (0.65 Å) <  $Ni^{2+}$  (0.69 Å). Similarly to what noted for the counter-ions B, the presence of A ions in mixed valence state cannot be ruled out altogether and this would explain some discrepancies observed between the three different series, with respect to the aforementioned sequence of A ion size. In particular, a small  $V^{3+}$  (0.64 Å) fraction can be present, whereas the large spread of the Mn-doped pigments suggests that a

significant amount of  $Mn^{2+}$  (0.83 Å) can also enter the rutile structure, in agreement with the UV-Vis-NIR spectra. A similar spread is observed for Cr, although the occurrence of  $Cr^{2+}$  (0.80 Å) in CN appears unlikely for this metal ion.

The detailed analysis of the distortions induced in the rutile structure by the incorporation of different ions and counter-ions is still under study. Figure 7 shows the variation of the apical vs. the square planar bond distances in the  $TiO_6$  octahedron for the studied pigments.

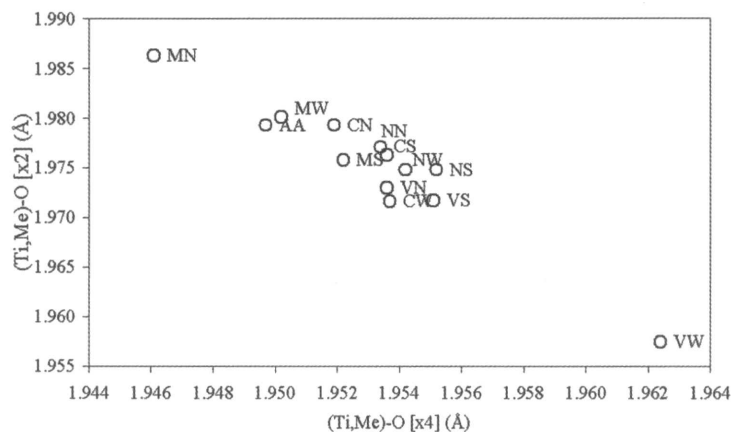


Figure 7. Plot of the apical vs. square planar bond distances of the  $(Ti,Me)O_6$  octahedron in rutile.

The common trend indicates that doping by different ions induces a general decrease of the octahedral elongation and enlargement of the square basal plane of the octahedron with respect to the reference rutile sample (AA). This is consistent with the general increase of the average bond distances and cell volumes, with respect to reference rutile sample as shown on Figure 8.

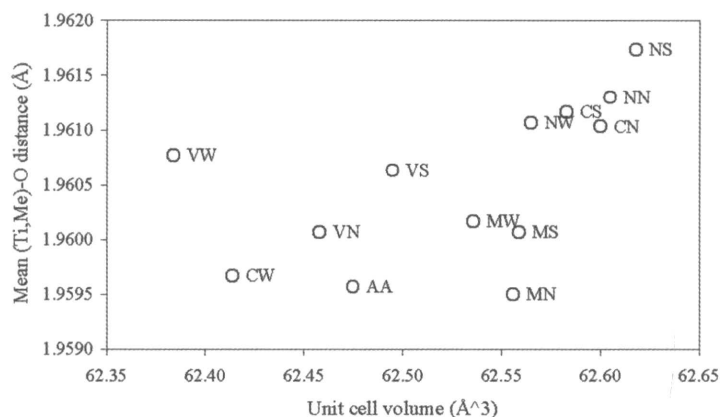


Figure 8. Plot of the mean  $(Ti,Me)-O$  bond distance vs. the unit cell volume.

Considering the commonly used formula which relates, for a given ion, the crystal-field parameter ( $\Delta_o$ ) to the average bond distance of the coordination shell ( $d$ )

through a constant ( $k$ ),  $\Delta_o = k/d^5$ , it might be predicted a significant decrease of the crystal-field parameter for most of the doped rutile pigments in this study, compared to the standard undoped rutile.

#### 4. CONCLUSIONS

This work has been carried out on rutile based pigments prepared in 12 different compositions with the stoichiometry  $Ti_{1-2x}A_xB_xO_2$  - where  $A = Cr, Mn, Ni, V$ ;  $B = Nb, Sb, W$  ( $x=0.03$ ) - and fired at 5 different temperatures (700, 800, 900, 1000, 1100 °C). A combination of X-ray powder diffraction, Rietveld refinement and UV-Vis-NIR spectroscopy has been used for pigment characterization. Concerning the influence of the metal transition ions on the anatase-to-rutile transition rate, it has been found that V is the most effective ion in promoting the transition, followed by Cr, Ni and Mn. Besides, the influence of counter-ions Sb and W, and the known retarding effect of Nb were found to be completely hidden by the effect of the transition metal ions. The anatase-to-rutile transition is important for the colour properties since the  $Ti^{4+}$ -O charge transfer band partially shifts from the UV to the visible region, being then partially superimposed on the transition metal ions absorption spectra. This explains to some extent the proportionality of the increase in colour intensity with respect to the rutile content of synthesized pigments. The analysis of the UV-Vis-NIR spectra and the structural results from Rietveld refinements on samples fired at 1100 °C have allowed gaining some insights into the valence state of the incorporated dopant ions and counter-ions. We suggest that the  $c$  unit cell dimension is mainly affected by varying the counter-ions size, according to a sequence  $W < Nb < Sb$ . The control exerted by incorporation of the transition metal ions, mainly on the increase of the  $a$  unit cell dimension, is less straightforward; the derived sequence of ionic size  $V < Cr < Mn < Ni$  can be regarded as a rough approximation. Preliminary analysis of the refined bond lengths shows a general decrease of the  $TiO_6$  octahedral elongation and increase of mean bond lengths induced by doping the rutile structure; this would imply a decrease of the crystal-field parameter ( $\Delta_o$ ) for a given ion, with respect to the undoped rutile.

#### REFERENCES

- [1] R. Loughbrough, TiO<sub>2</sub> pigment, Overcapacity hits again, *Industrial Minerals*, 6 (1992) 37-53.
- [2] R. Ren, Z. Yang, L. L. Shaw, Polymorphic transformation and powder characteristics of TiO<sub>2</sub> during high energy milling. *J. Mat. Sci.* Vol. 35, 23 (2000) 6015-6026.
- [3] S. A. Selim, Ch. Philip, S. Hanafi, H. P. Boehm, Effect of thermal treatment on the structure and texture of titania, *J. Mat. Sci.* Vol. 25, 11 (1990) 4678-4687.
- [4] H. Zhang, J. F. Banfield, Phase transformation of nanocrystalline anatase-to-rutile via combined interface and surface nucleation, *J. Mater. Res.* Vol 15, 2 (2000) 437-448.
- [5] R.D. Shannon J.A. Pask, Kinetics of the anatase to rutile transformation, *J. Am. Ceram. Soc.* Vol. 48 (1965) 391-398.
- [6] M. Sacerdoti, M.C. Carotta, L. Crema, G. Martinelli, Sol-gel processed TiO<sub>2</sub>-based nano-sized powders for use in thick film gas sensors for atmospheric pollutant monitoring, *J. Sol-Gel Tech.* 22 (2001)167-79,
- [7] A. S. Marfunin, *Physics of Minerals and Inorganic Materials*, Springer-Verlag Berlin Heidelberg New York 1979.
- [8] *Colour, pigments and colouring in ceramics*, Società Ceramica Italiana Ed. 2003
- [9] S. Ishida, M. Hayashi and Y. Fujimura, Spectroscopic study of the chemical state and coloration of chromium in rutile, *J. Am. Ceram. Soc.*, 73, 11 (1990) 3351-3355.
- [10] R. A. Eppler, Niobium and tungsten oxides in titania-opacified porcelain enamels, *Cer. Bull.* Vol. 52, 12 (1973) 879-880.

- [11] The DCMA Classification System of the Complex Inorganic Color Pigments
- [12] R. Rodrigues-Talavera, S. Vargas, R. Arroyo Murillo, R. Montiel-Campos and E. Haro-Poniatowski, Modification of the phase transition temperatures in titania doped with various cations, *J. Mater. Res.* Vol. 12, 2 (1997) 439-443.
- [13] S. Hishita, I. Mutoh, K. Koumoto and H. Yanagida, Inhibition mechanism of the anatase-to-rutile phase transformation by rare earth oxides, *Ceramics International*, Vol. 9, 2 (1983) 61-67.
- [14] L.E. Depero, P. Bonzi, M. Zocchi, C. Casale, G. de Michele, Study of the anatase-rutile transformation in TiO<sub>2</sub> powders obtained by laser-induced synthesis, *J. Mater. Res.* Vol. 8, 10 (1993) 2709-2715.
- [15] R.A Eppler., Effect of antimony oxide on the anatase-rutile transformation in titanium dioxide, *J.Am. Ceram. Soc.*, Vol. 70, 4 (1987) C64-C66.
- [16] G. Croft, M. J. Fuller, Crystalline oxidic solid solutions of Tin (IV) and Titanium (IV), their coloration by and thermal reaction with some metal ions. Part 1: The rutile Sn<sub>x</sub>Ti<sub>(1-x)</sub>O<sub>2</sub> system and its interaction with V(V), Cr(III), Cr (IV), Mn (III), Fe (III), Co (II), Ni (II), CU (II) and Sb (III). *Br. Ceram. Trans.* 78, 3 (1979) 52-56.
- [17] F. Ren, S. Ishida, N. Takeuchi, M. Wakamatsu, Colors of chromium in SnO<sub>2</sub>-TiO<sub>2</sub> bases systems, *Ceram. Eng. Sci. Proc.* 13 [1-2] (1992) 132-138.
- [18] F. Matteucci, G. Cruciani, M. Dondi, G. Guarini, M. Raimondo, in preparation.
- [19] Y. Tanabe, S. Sugano, On the absorption spectra of complex ion, *J. Phys. Soc. Japan* 9 (1954) 753-766 and 766-780.
- [20] R. D. Shannon, Revised effective ionic radii and systematic studies of interatomic distances in halides and chalcogenides. *Acta Cryst.*, A32 (1976) 751-767.